



HOT TENSILE PROPERTIES OF AUTOGENOUS GAS TUNGSTEN ARC WELDED AISI 304HCu SUPER AUSTENITIC STAINLESS STEEL JOINTS

*Vinoth Kumar M¹, Balasubramanian V² and Gourav Rao A³

¹Research Scholar, Department of Manufacturing Engineering, Annamalai University, Annamalainagar – 608 002, Tamilnadu, India.

²Center for Materials Joining and Research (CEMAJOR), Department of Manufacturing Engineering, Annamalai University, Annamalainagar – 608 002, Tamilnadu, India.

³Naval Materials Research Laboratory (NMRL), Ambarnath, Mumbai - 421 506, India.

ABSTRACT

The USC boilers operate at higher steam temperature and pressure which in turn increase the efficiency of the power plant. The recently developed AISI 304HCu austenitic stainless steel with nominal composition of 0.1C-18Cr-9Ni-3Cu-Nb-N is listed as a candidate material for superheaters and reheaters in the U.S program for development of materials for USC with steam temperatures of 760 °C. Welding may cause the changes in microstructure and result in local compositional variation due to segregation, which alters the solidified phases in room temperature and may affect the mechanical properties. The hot tensile properties of autogenously gas tungsten arc welded AISI 304HCu austenitic stainless steel tubes were evaluated. Autogenous welding of AISI 304HCu resulted in inferior weld joint with tensile strength lower than the parent metal both at room temperature and high temperatures.

Keywords: AISI 304HCu Austenitic stainless steel, Gas Tungsten Arc welding, Hot tensile properties and Microstructure.

1. Introduction

The growing concern on emission of green house gases and reduction in coal consumption has increased the phase to set up ultra super critical (USC) boilers. The USC boilers operate at higher steam temperature and pressure which in turn increase the efficiency of the power plant. The increase in efficiency results in better utilization of the coal and reduction of “carbon foot print” per MW of power generated [1-3].

Austenitic stainless steels are the candidate material for the super heaters and reheaters in the boilers where oxidation and fire side corrosion resistance is a major concern, in addition to the creep strength. The recently developed AISI 304HCu austenitic stainless steel with nominal composition of 0.1C-18Cr-9Ni-3Cu-Nb-N is listed as a candidate material for super heaters and reheaters in the U.S program for development of materials for USC with steam temperatures of 760 °C [4]. AISI 304HCu derives its excellent creep strength from its distinct Cu addition which precipitates as fine Cu rich particle under creep conditions, in addition to NbCrN, Nb(C,N) and M₂₃C₆ particles [5].

In boiler construction welding is considered as the major manufacturing process, in particular gas tungsten arc (GTA) welding is employed for fabrication of boiler tubes. Welding can alter the microstructure and phase balance of the material which may affect the mechanical properties.

In particular under non-equilibrium cooling conditions, such as welding, highly alloyed steels such as AISI 304HCu may result in local compositional variation due to segregation, which alters the solidified phases in room temperature. From literature survey [6-11], it is found that the published work on autogenous welding of AISI 304HCu is very scant. Hence in this work, it is planned to study the effect of autogenous GTA welding on microstructure and hot tensile properties of AISI 304HCu austenitic stainless steel tubes.

2. Experimental Details

The chemical composition and mechanical properties of the AISI 304HCu tubes (outer diameter 57.1 × 3.5 mm thick) in as-received condition are given in Table 1 and 2 respectively. The joint with square butt preparation, without root gap, was welded using GTAW process. Argon was used as the shielding and purging gas. The welding parameters used in this investigation are shown in Table 3. The photograph of the autogenously GTA welded joint is shown in Fig 1a. The metallographic samples were prepared using standard metallographic techniques and etched with Glyceregiafor 5-10 s to reveal the general structure of parent metal and with boiling Murakami's reagent to reveal δ ferrite and carbides in the weld metal.

*Corresponding Author - E- mail: vinothmecho@gmail.com

Table 1. Chemical composition (wt %) of as received AISI 304HCu tubes

C	Si	Mn	P	S	Cr	Ni
0.086	0.23	0.81	0.021	0.0003	18.18	9.06
N	Cu	Nb	Mo	B	Al	
0.095	3.080	0.045	-	0.0039	0.01	

Table 2. Mechanical properties of AISI 304HCu

0.2% Yield strength (MPa)	Ultimate tensile strength (MPa)	Elongation in 25mm gauge length (%)	Annealing temperature (°C)
284.2	575.8	71.8	1145

Table 3. Parameters used for autogenous GTA welding of AISI 304HCu

Power source type	Constant Current
Current (A)	100
Voltage (V)	11
Welding speed (mm/min)	70
Heat input (kJ/mm)	0.943

The microstructural examination of the samples was carried out using light optical microscope (OM), Scanning Electron Microscope (SEM) and the compositional variation within the weld regions were analysed using Energy Dispersive Spectroscopy (EDS) attached with SEM. The δ ferrite measurements in the welds were carried out using Ferritoscope. The specimens for transverse tensile test were extracted from the weld joints using wire-cut electric discharge machining. Fig 1b represents the dimension of the transverse tensile specimens extracted from the weld joints.

Tensile test was carried out using a Instron make universal testing machine (UTM), at a nominal strain rate of $1 \times 10^{-3} \text{ S}^{-1}$. The tensile tests were carried out at four different temperatures, such as room temperature (RT), 550°C, 600°C, and 650°C. The UTM system was equipped with a three-zone resistance heating furnace for high temperature tests and a computer with data acquisition system for obtaining digital load-elongation data. The photograph of hot tensile test specimens before and after test was shown in Fig. 1c and 1d respectively. The hardness was measured along the weld center line using Vickers microhardness tester with a load of 500 g and dwell time of 15 s. The fracture surfaces of the tensile specimens was analysed using SEM to reveal the mode of fracture.

3. Results

3.1 Microstructure

The Fig 2a shows the macrograph of the autogenous GTA weld joint which reveals the various regions across the joint, consisting of parent metal (PM), heat affected zone (HAZ), Fusion zone (FZ). The micrograph of weld center is shown in Fig 2b, which reveals the presence of cellular austenite grains with intercellular δ ferrite (marked by arrow). The micrograph of the weld center etched with murakami is shown in Fig 2c, reveals the presence of intercellular and interdendritic eutectic delta ferrite segregation in the weld. The Fig 2d shows the delta ferrite and carbide segregation in the fusion line of the weld.

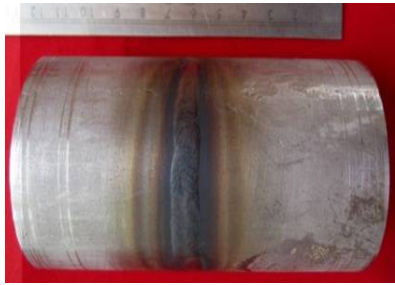
In order to determine the type of precipitates available within δ ferrite the sample was etched with murakami's reagent near boiling point. Murakami's reagent preferentially etches the carbides at the austenite grain boundaries and δ ferrite. The SEM micrograph of weld metal is shown in Fig 3a, reveals the presence of precipitates within the intercellular and interdendritic ferrite phase (marked by arrow). The composition of the δ ferrite region was revealed by EDS analysis of the spot (S1) and found to be rich in Fe, Cr, B, and C, which reveals the presence of $\text{M}_{23}(\text{C},\text{B})_6$ borocarbides [12,13] within the delta ferrite stringers.

3.2 Ferrite measurement

The δ ferrite content in the weld metal was measured using ferrite scope and the average ferrite content was found as 1.57 %. The amount of δ ferrite determined using the ferrite scope was much lower than volume of dark phase (termed as δ ferrite) present in the SEM micrograph of Fig. 2c. This is attributed to the presence of borocarbides and the eutectic's segregated within the delta ferrite stringers, thus the grey area etched by murakami's reagent is a eutectic mixture of borocarbides and δ ferrite.

3.3 Tensile properties

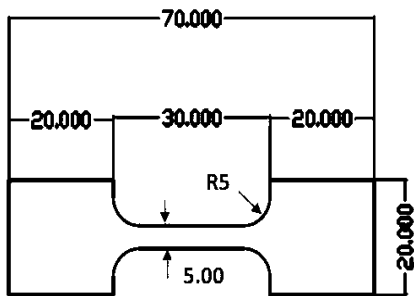
The engineering stress-strain curves of parent metal and autogenous weld joint at various test temperatures are shown in Fig. 4a and 4b respectively and the tensile properties are presented in Table 4. The RT tensile strength of autogenous GTA weld joint is lesser than the PM strength (-2 %), with failure located in the weld center. The strength and elongation values of both parent metal and autogenous weld joints decreased with increase in test temperature. The tensile strength decreases by 30 % for parent metal and by 31 % for autogenous weld joint with increase in test temperature from RT to 650 °C.



a. Autogenously welded tube joint



b. Hot tensile specimens before test

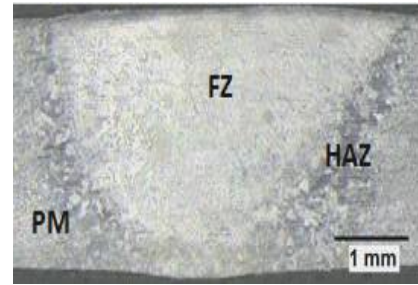


c. Dimensions of hot tensile specimen in 'mm'

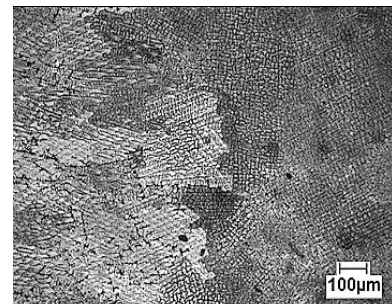


d. Hot tensile specimens after test

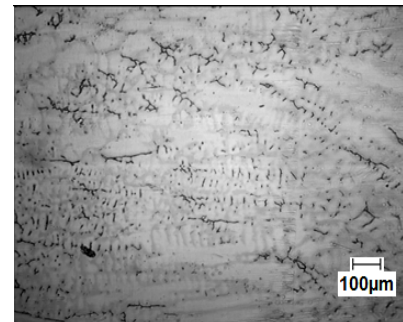
Fig. 1 Photograph of welded tubes and tensile specimens



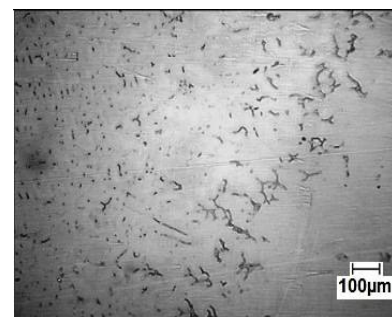
a. Macrograph



b. Weld metal (Aquaregia)



c. Weld metal (Murakami's)

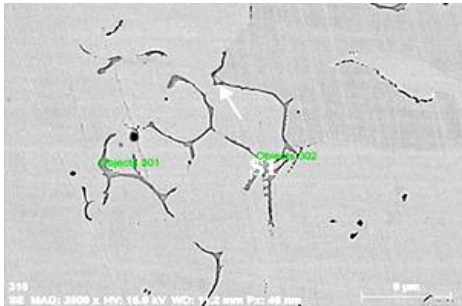


d. Fusion line (Murakami's)

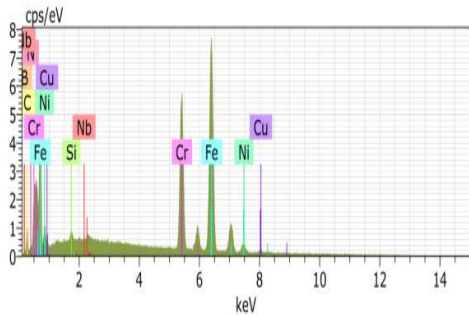
Fig. 2 Optical micrograph of autogenous GTA weld joint

3.4 Hardness

The mid-thickness micro hardness survey across the autogenous weld joint is shown in Fig. 5. The hardness variations observed within the weld metal region was attributed to the presence of ferrite and borocarbides segregated to the interdendritic and intercellular boundaries. The lowest hardness value was recorded in the weld metal of the autogenous weld joint, where the failure of tensile specimen was reported. The HAZ region hardness value is equivalent to that of the parent metal hardness value 175 HV.

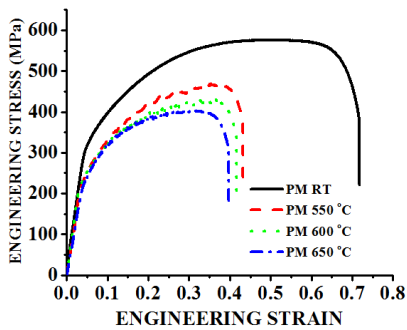


a. Weld metal (Murakami's)

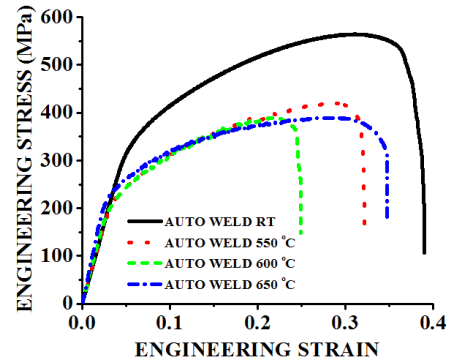


b. Spot EDS of grey region in Fig. 3a

Fig. 3 SEM micrograph and EDS analysis of autogenous GTA weld joint



a. Parent metal



b. Autogenous weld joints

Fig. 4 Engineering stress-strain curves of AISI 304HCu

Table 4. Tensile properties of parent metal and autogenous GTA weld joints of AISI 304HCu

	Test temperature (°C)	0.2% Yield strength (MPa)	Ultimate tensile strength (MPa)	Elongation in 25 mm gauge length (%)	Failure location
Parent metal (PM)	RT	284.2	575.8	71.8	-
	550	205.5	465.8	43.0	-
	600	193.0	431.8	41.7	-
	650	204.3	401.8	39.6	-
Autogenous weld joint	RT	302.4	564.3	38.96	WM
	550	201.6	420.4	32.09	WM
	600	173.0	388.2	24.97	WM
	650	206.2	389.0	34.70	WM

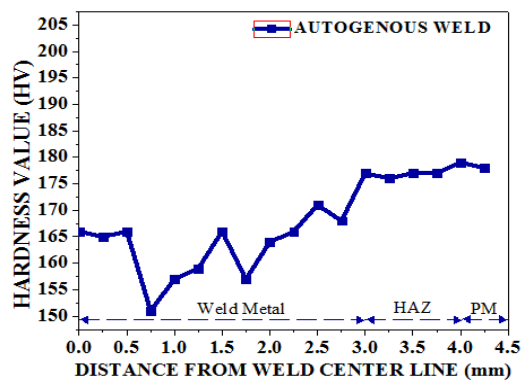
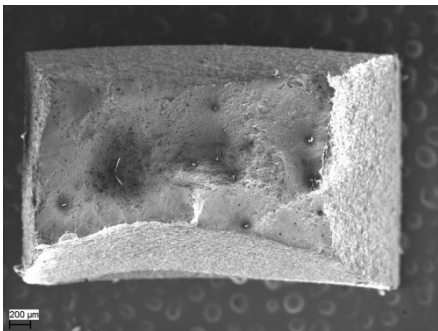


Fig. 5 Hardness survey across the weld center line

3.5 Fracture Surfaces

The macrograph of fracture surface and SEM fractographs of parent metal and autogenous weld joint tested at RT and 550°C are shown in Fig. 6 and Fig. 7 respectively. The SEM macrograph of both parent metal and weld joint tested at RT (refer Fig. 6a and 6b) reveals considerable amount necking prior to fracture, while the specimen tested at 550 °C does not reveal such feature (refer Fig. 6c and 6d). The RT fractograph of parent metal at higher magnification is shown in Fig. 7a, invariably consists of voids of varying sizes surrounded by fine dimples, voids are associated with the precipitates present in the austenitic matrix of PM.



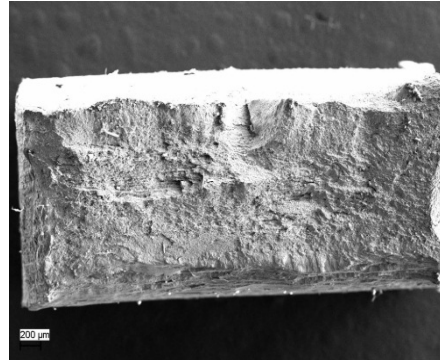
a. Parent metal (Room Temperature)



b. Autogenous weld joint (Room Temperature)



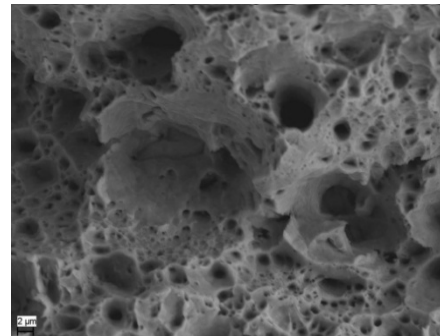
c. Parent Metal (550°C)



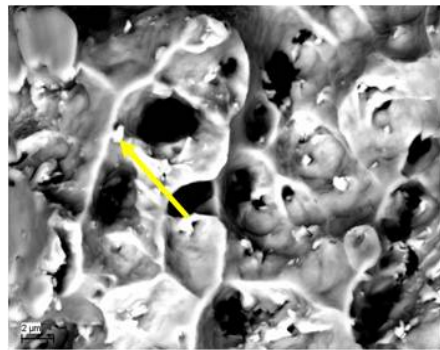
d. Autogenous weld joint (550°C)

Fig. 6 Macrograph of fracture surface

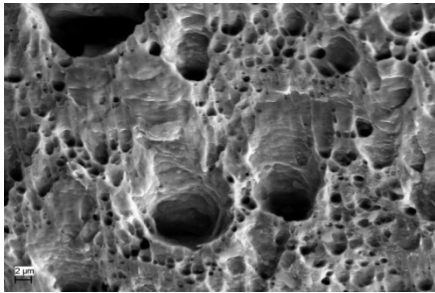
The fracture surface of PM tested at high temperature (550 °C) reveals fewer voids, much larger in size and cleavage like featureless facets than the fracture surface of PM tested at RT [14]. It is evident from the fractographs that the fracture of PM at high temperature failed in more brittle than the PM tested at RT.



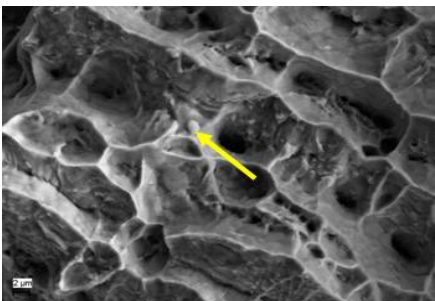
a. Parent metal (Room Temperature)



b. Autogenous weld joint (Room Temperature)



c. Parent Metal (550°C)



d. Autogenous weld joint (550°C)

Fig. 7 SEM fractographs

The more brittle nature of failure in high temperature test is evidenced by the constant decrease in elongation of the specimens with increase in test temperature. The high magnification SEM fractograph of autogenous joints tested at RT and 550 °C is shown in Fig. 7b and 7d, the dendritic cast structure of the weld metal. Since the fracture of the autogenous joints was located in the elongated voids closely matches the dendritic size of the weld metal. The precipitates segregated along the dendritic boundaries (marked by arrow) acts as the crack initiation sites.

4. Discussion

The WRC-1992 diagram is commonly used to predict the mode of solidification and the amount of residual delta ferrite in the weldments. The Cr and Ni equivalents calculated for AISI 304HCu are 18.2 and 17.7 respectively, which falls in the region of austenitic mode of solidification with no residual delta ferrite. The weld metal consists of 0.78 % δ ferrite, which in contrary to the predicted weld metal composition. The weld solidifies by epitaxial growth and a plane front solidification zone near the fusion line, and transforms to cellular mode with micro segregation to the cellular boundaries [15].

The segregation of Fe, Cr, B, C (refer Fig 3b) in the intercellular region of the austenite reveals the

presence of $M_{23}(C,B)_6$ borocarbides [12,13]. The limited solubility of B in austenitic stainless steel causes the excess B to segregate along the grain boundaries and combine with Cr and Fe to form a low melting eutectic with the austenite [16]. The presence of $M_{23}(C,B)_6$ borocarbides in the weld metal acts as the crack initiation sites in the fracture during tensile testing, with austenitic weld metal free of elemental boron results in lesser hardenability of the joint.

The failure of weld joint was located at weld center regardless of test temperature, which recorded the lowest hardness in the weld joint (refer Fig 7). In single pass autogenous weld, the weld metal solidifies as coarse columnar grains by epitaxial growth towards the weld center with preferential orientation, may results in a weak centerline in the weld [17]. The reduction in the strength values of parent metal and weld joints with increase in test temperature is attributed to the accelerated recovery process [18].

5. Conclusions

1. Autogenous GTA welding of AISI 304HCu resulted in inferior tensile strength of the joint, lower than the parent metal both at room temperature and high temperatures (550 – 650 °C).
2. The inferior tensile strength of the autogenously GTAW joints of AISI 304HCu austenitic stainless steel is attributed to the segregation of the alloying elements to form borocarbides and the weak center line of the single pass autogenous welds.
3. Autogenous GTA welding of AISI 304HCu is not suitable for high temperature applications, as the failure was located in the weld metal of the joints and the delta ferrite in the weld metal may transform to sigma phase during operation at high temperatures.

Acknowledgements

The authors wish to express their sincere thanks to M/s Mailam India Ltd, Pondicherry, India for providing financial assistance to carry out this research work through the Mailam India Research (MIR) Fellowship, M/s Salzgitter Mannesmann Stainless Tubes Italia Srl of Italy for supplying the AISI 304HCu tubes required to carry out this work, The Director, Naval Materials Research Laboratory, Ambernath, Mumbai for providing the facility to carry out hot tensile testing and Dr. N. Murugan, Professor, Department of mechanical engineering, Coimbatore Institute of Technology, Coimbatore for his help rendered in ferrite measurement.

References

1. Brozda J (2007), "New generation austenitic steels used in supercritical power industry plant", *Journal of Welding International*, Vol.21, 512-520.
2. Shuping Tan Zhen hua Wang Shi chang Cheng (2010), "Hot deformation behavior of Super304H austenitic heat resistant steel", *Journal Minerals Metallurgy Materials*, Vol. 17, 167-172.
3. David S A Siefert J A Feng Z (2013), "Welding and weldability of candidate ferritic alloys for future advanced ultrasupercritical fossil power plants", *Journal of Science and Technology of Welding and Joining*, Vol.18, 632-651.
4. Viswanathan R Henry J F Tanzosh J (2005), "U.S. program on materials technology for ultra-supercritical coal power plants", *Journal of Materials Engineering and Performance*, Vol.14, 281-292.
5. Xinmei Li Yong Zou Zhong wen Zhang and Zengda Zou (2010), "Microstructure evolution of a novel super304H steel aged at high temperatures", *Journal of Materials Transactions*, Vol.51, 305-309.
6. IndraniSen Amankwah E Kumar N S (2011), "Microstructure and mechanical properties of annealed SUS 304H austenitic stainless steel with copper", *Journal of Material Science and Engineering A*, Vol. 528, 4491-4499.
7. Huachun Yang FangfangPeng Xiaoling Miao and Xiaochuan Yang (2006), "Investigation of the aging behavior on boiler steel tube super304H", *Journal of Pressure Equipments and System*, Vol. 4, 96-99.
8. Xinmei Li Yong Zou Zhong wen Zhang (2010), "Microstructure evolution of a novel super 304H steel aged at high temperatures", *Journal of Material Transactions*, Vol.51, 305-309.
9. Bai J W Liu P P Zhu Y M (2013), "Coherent precipitation of copper in Super 304H austenite steel", *Journal of Material Science and Engineering*, Vol. (A) 584, 57-62.
10. Vu The Ha Woo Sang Jung (2012), "Creep behavior and microstructure evolution at 750 °C in a new precipitation strengthened heat resistant austenitic stainless steel", *Journal of Material Science and Engineering A*, Vol. 558, 103-111.
11. Vekeman J Huysmans S De Bruycker E (2014), "Weldability assessment and high temperature properties of advanced creep resisting austenitic steel DMV304HCu", *Journal of Welding in the World* Vol. 58, 873-882.
12. Hoffman J P De Jesus ASM (1989), "The distribution of boron in stainless steels as revealed by a nuclear technique", *Journal of South African Institute of Minerals and Metal*, Vol.89, 81-87.
13. Karlsson L Andren H O Nord H (1982), "Grain boundary segregation in austenitic stainless steel containing boron - an atom probe study", *Journal of Scripta Metallurgica*, Vol. 16, 297-302.
14. Afrin N Chen D L Cao X (2007), "Strain hardening behavior of a friction stir welded magnesium alloy", *Journal of Scripta Matereilia*, Vol. 57, 1004-1007.
15. Elmer J W Allen S M Eagar T W (1989), "Microstructural development during solidification of stainless steel alloys", *Journal of Metallurgical Transactions A*, Vol. 20, 2117-2131.
16. Gary M Carinci (1994), "Grain boundary segregation of boron in an austenitic stainless steel", *Journal of Applied Surface Science*, Vol. 76, 266-271.
17. Villafuerte J C Kerr H W (1990), "Grain structures in gas tungsten-arc welds of austenitic stainless steels with ferrite primary phase", *Journal of Metallurgical Transactions A*, Vol. 21, 979-986.
18. Choudhary B K RaoPalaparti D P (2012), "Comparative tensile flow and work hardening behaviour of thin section and forged thick section 9Cr-1Mo ferritic steel in the framework of voce equation and Kocks-Mecking approach", *Journal of Nuclear Materials*, Vol. 430, 72-81.

Nomenclature

Symbol	Meaning	Unit
RT	Room temperature	° C
wt	weight	%